



Constraints on crust-mantle transition zone with Pn waveforms: A case study of eastern China and southern Korean Peninsula



Shiban Ding^a, Sida Ni^{b,*}, YoungHee Kim^c, Xiaohui He^d

^a School of Earth and Space Science, University of Science and Technology of China, Hefei 230026, China

^b State Key Laboratory of Geodesy and Geodynamics, Institute of Geodesy and Geophysics, Chinese Academy of Sciences, Wuhan 430077, China

^c School of Earth and Environmental Sciences, Seoul National University, Seoul 08826, Republic of Korea

^d Guangdong Provincial Key Lab of Geodynamics and Geohazards, School of Earth Sciences and Engineering, Sun Yat-Sen University, Guangzhou 510275, China

ARTICLE INFO

Keywords:

Crust-mantle transition zone (CMTZ)
Velocity gradient
Pn waveform
Waveform modeling
Eastern China
Southern Korean Peninsula

ABSTRACT

The seismic velocity structure of the crust-mantle transition zone (CMTZ) provides key constraints on crustal dynamics, and can be studied with Pn wave which propagates horizontally along the Moho discontinuity. In this study, we first explore an effect of velocity-gradient structures in the CMTZ through synthetic Pn waveforms, and demonstrate that the shape of Pn changes from step-like to pulse-like when the CMTZ becomes from sharp to a gradient velocity structure, respectively. We then use Pn waveforms of the regional earthquakes (the July 2012 Mw 4.8 earthquake in east China and the September 2016 Mw 5.1 earthquake in South Korea) to examine the CMTZ structures to the west and east of the Yellow Sea and thus to constrain tectonic affinity between the eastern China and southern Korean Peninsula. The Pn waveforms from the Mw 4.8 event in east China show that the Moho in southern Yangtze Craton is sharp whereas there may be a gradient structure in CMTZ with a 6–10 km thickness in northern Yangtze Craton. The Pn waveforms from the Mw 5.1 event in South Korea show that the CMTZ in South Korea is also sharp, similar to the southern Yangtze Craton. Observed difference in CMTZ structures suggest that Sulu Orogenic Belt may extend along the north of the Gyeonggi Massif in Korea.

1. Introduction

The characteristics of continental Moho discontinuity play an important role in understanding the tectonic evolution and dynamic process in the Earth's interior (Hale and Thompson, 1982; Morozov et al., 2001; Abbott et al., 2013; Carbonell et al., 2013; Hawkesworth et al., 2013). Seismic profiling and petrological studies suggested that the crust-mantle interface cannot be just a simple boundary between the felsic-mafic crust and the ultra-mafic upper mantle (e.g., Mengel and Kern, 1992; Prodehl and Mooney, 2012; O'Reilly and Griffin, 2013; Thybo and Artemieva, 2013; Mjelde et al., 2013). It is likely to be a transition zone which is more appropriately called crust-mantle transition zone (CMTZ) (Owens and Zandt, 1997; Carbonell et al., 2002; Lin and Wang, 2005; Zheng et al., 2006).

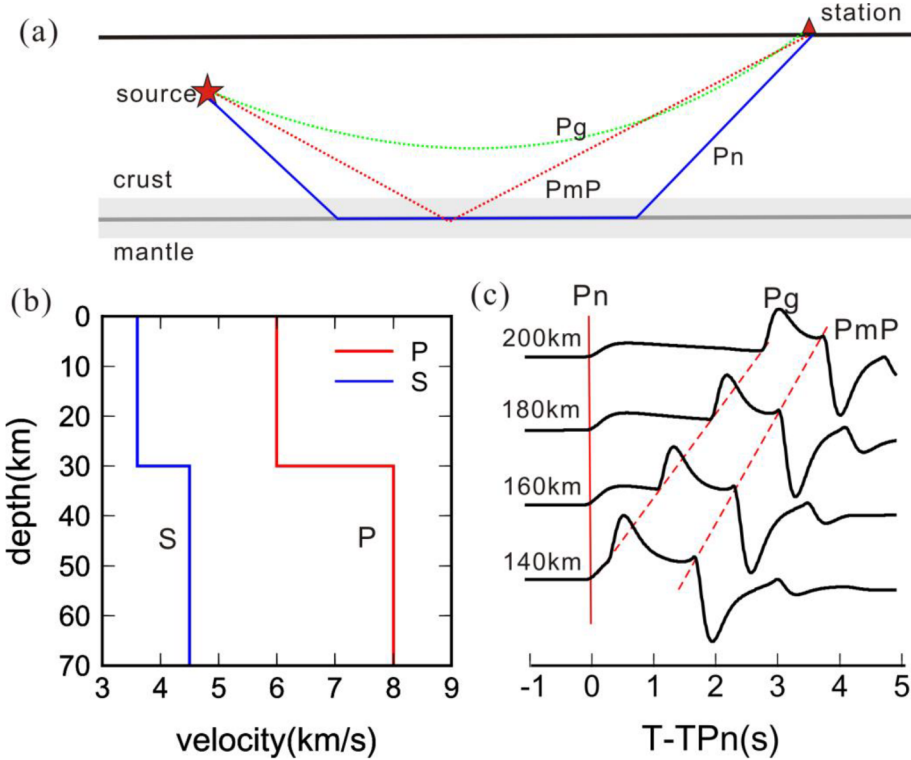
There are various approaches in studying velocity structures of CMTZ (e.g., Brun and Gutscher, 1992; Cook, 2002; Gao et al., 2000; Niu and James, 2002; Chang and Baag, 2007; Zhang et al., 2011; Teng et al., 2013). Deep seismic reflection method typically provides relatively high resolution, which is usually on the order of km (Flecha et al., 2009; Palomeras et al., 2009, 2011; Tian et al., 2014). With the teleseismic

receiver function method, the ray is almost vertically incident and is thus sensitive to the CMTZ velocity structure beneath stations. Whereas, the ray path of Pn is travelling mostly horizontal along the crust-mantle boundary (Fig. 1a), and thus Pn is most sensitive to the CMTZ velocity structure between earthquake source and stations (Savage et al., 2003; Liang et al., 2004; Li et al., 2012).

Pn travel-time tomography has been used extensively to retrieve crust and upper mantle velocity structures in various regions (e.g., Hole, 1992; Di Stefano et al., 1999; Uhlmann, 2001; Xu et al., 2002; Al-Lazki et al., 2004; Hearn et al., 2004; Li et al., 2006; Pei et al., 2007; Tian et al., 2009; Myers et al., 2010; Wang et al., 2013a, 2013b; Sun and Kennett, 2016; Buehler and Shearer, 2017). The travel time of Pn is sensitive to the variation of Moho depth and the velocity of the uppermost mantle, while Pn amplitudes are greatly affected by gradient velocity structure near Moho (Braile and Smith, 1975; Yang et al., 2007; Xie and Lay, 2016). Instead, the information of Pn waveform may provide independent constraints on velocity structure near CMTZ. For example, Savage et al. (2003) analyzed Pn waveform complexity and proposed a model to describe the velocity structure around the Southern Sierra Nevada and Walker Lane CMTZ through finite-difference (FD) waveform modeling.

* Corresponding author.

E-mail address: sdni@whigg.ac.cn (S. Ni).



As the rapid development of numerical methods (Komatitsch and Tromp, 1999; Zhu and Rivera, 2002; Zhang et al., 2012; Li et al., 2014) and increasing number of regional seismic stations, Pn waveform modeling can be applied in other regions.

There is a spectacular tectonic landscape with faults, orogen and suture in east Asia associated with the collision of Sino-Korea plate and Yangtze plate during Permian and Triassic (Yin and Nie, 1993; Zhang, 1997). Tectonic affinity between eastern China and southern Korean Peninsula (Chang and Baag, 2007; Yoo et al., 2007) is essential for understanding the tectonic frame of east Asia, and it has been a controversial topic of debate due to limited deep structural information (Yin and Nie, 1993; Zhang, 1997; Chang and Park, 2001; Oh et al., 2006; Hao et al., 2007; Zhai et al., 2007; Tang et al., 2010). The seismicity surrounding the Yellow Sea has been mild with earthquake magnitude typically less than 5.0 (Hong and Choi, 2012) until 2016. In particular, there have been three moderate-size ($M_w > 5.0$) earthquakes in South Korea since 2016 (Kim et al., 2016, 2017, 2018). The dense regional network records of these earthquakes make it possible to examine the deep seismic structure, such as CMTZ, thus providing constraints on the tectonic affinity between eastern China and southern Korean Peninsula.

In this study, we first examine the effect of various velocity structures in the CMTZ on Pn waveforms using synthetic tests, and then constrain the CMTZ structure to the west and east of the Yellow Sea using Pn waveforms from two regional earthquakes. The similarity of CMTZ in these regions is discussed to provide an insight into the tectonic affinity between Korean Peninsula and eastern China.

2. Pn waveform forward modeling

There are various methods for calculating synthetic waveforms, which include integral transformation methods (Yao and Harkrider, 1983; Wang, 1999; Zhu and Rivera, 2002), ray methods (Helmberger, 1968; Chapman, 1978) and numerical methods such as FD and spectral-element method (SEM) (Vidale and Helmberger, 1988; Komatitsch and Tromp, 1999). We use the frequency-wavenumber (FK) method to generate synthetics in this study (Zhu and Rivera, 2002). Pn waveforms

Fig. 1. Models and schematics to illustrate seismic phases to constrain the crust-mantle transition zone (CMTZ). (a) A diagram showing seismic ray paths for Pn, Pg, and PmP in a simplified structure for the crust and mantle. (b) Seismic velocity model, for a 30 km-thick crust and mantle. (c) Synthetic vertical displacement waveforms including Pn, Pg, and PmP (red solid and dashed lines, respectively) computed from the model in (b). The explosion source is placed at 10 km depth, and its source duration time is 1 s. The waveforms for different distances (number shown on the left of each waveform) are aligned on the theoretical arrival time of Pn.

on radial and vertical components typically show similar characteristics in synthetic waveforms. However, Pn on the vertical component often displays higher signal-to-noise ratio (SNR) in observed data, and thus we only select the vertical component data for our analysis. As isotropic explosion source is a good choice for simulating compressional wave, such as Pn, we therefore choose the explosion source to generate synthetics for Pn waveform modeling. The source is set to be at a depth of 10 km as most tectonic earthquakes occur in upper-middle crust, and their average depth is about 10 km (Scholz, 1998).

Fig. 1c shows synthetic waveforms with a velocity model which includes crust and mantle with a sharp CMTZ (Fig. 1b). Two phases, Pg and PmP arrive after the Pn arrival (Fig. 1c). Pn is partially overlapped with the subsequent Pg at the epicentral distance of 140 km (Fig. 1c). With a larger distance, the travel-time difference between Pn and the subsequently arriving Pg increases, and its difference is more than 2 s at 200 km. In order to isolate Pn from Pg, we choose the stations with distances larger than 200 km to analyze both synthetic and observed waveforms. Fig. 1c also shows that Pn displacement waveforms are step-like when the horizontal layered CMTZ is sharp (Fig. 1b), as expected for head waves which result in additional integral symbol in Eq. (1) in time domain as compared to turning waves which are essentially proportional to moment rate function (Aki and Richards, 2002).

Displacement of the Pn wave, u_{pn} , in time domain can be expressed as follows:

$$u_{pn}(t) = \int A \frac{\rho_1 \alpha_1^2}{\rho_2 \alpha_2 (1 - \alpha_1^2 / \alpha_2^2)} \frac{1}{r^{1/2} L^{3/2}} m(t - t_h) dt \quad (1)$$

where A represents coefficients to account for radiation pattern, t_h the arrival time of head wave, r the horizontal distance between source and receiver, and L the distance of the Pn path along the Moho. ρ_1 , ρ_2 , α_1 , and α_2 are density and P-wave velocity for crust and mantle, respectively. Usually, moment rate function $m(t)$ has a pulse-like shape, thus the waveform of Pn is step-like for sharp Moho due to the integration of a pulse-like shape.

We next explore the case where the CMTZ has a gradient structure. The CMTZ thickness can vary from < 2 km for a region with sharp

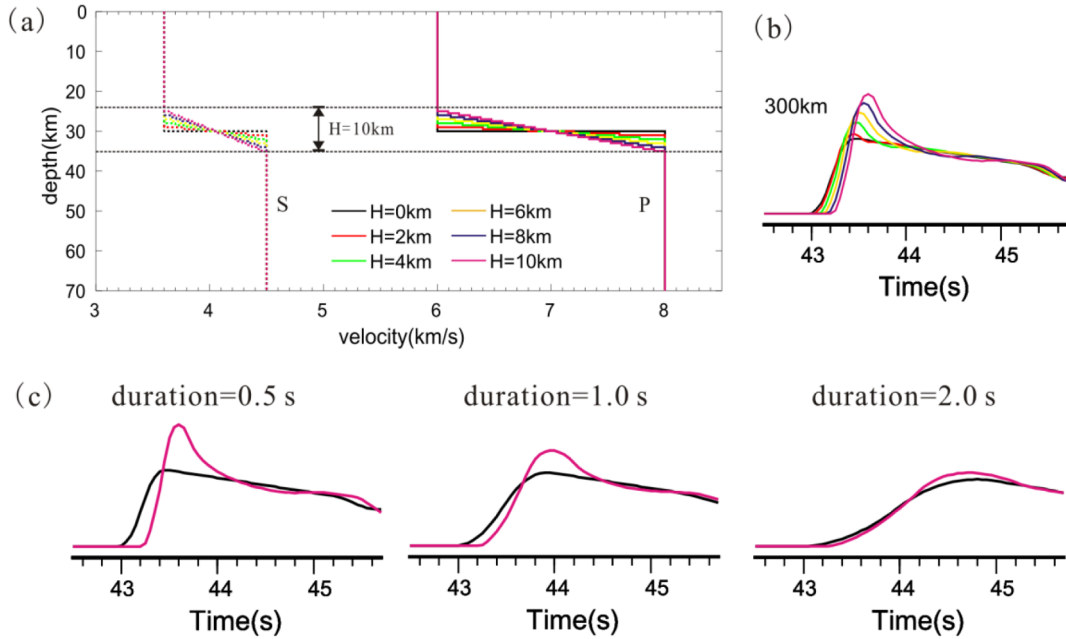


Fig. 2. The effect of positive gradient of CMTZ with its thickness (H) on Pn waveforms. (a) Seismic velocity models with variable velocity gradient of CMTZ and H of 0–10 km. (b) Synthetic vertical-component waveforms corresponding to the models in (a) with source durations of 0.5 s and epicentral distance of 300 km. (c) Synthetic vertical-component waveforms corresponding to different source durations (0.5 s, 1.0 s and 2.0 s) with 0–10 km thick CMTZ and epicenter distance of 300 km.

Moho (Niu and James, 2002), and up to 10 km (Prodehl, 1977; Owens and Zandt, 1985; Zheng et al., 2008). Taking these results, we consider the velocity of CMTZ as linearly increasing with its thickness in the range of 2–10 km (Fig. 2a). Since crustal and uppermost mantle velocities usually increase with depth with increasing pressure, we adopt cases with positive velocity gradient first (Fig. 2). An increasing thickness of the CMTZ causes a change in the waveform of Pn from step-like to pulse-like (Fig. 2b), and we see this consistent change in Pn waveforms for different distance (Fig. S1). The travel time of the pulse-like Pn is slightly delayed compared to the step-like Pn, and this may be caused by deeper Pn ray path for thickened CMTZ (Fig. 2b). We also test the cases for different source durations related to earthquakes with different magnitudes (Fig. 2c). The synthetics show that a pulse shape for the Pn waveforms is sharper for narrower source duration which has higher resolution for shorter wavelength (Fig. 2c). For the source duration of 2 s, which is expected for the duration time of Mw 5.5 earthquake (Gibson and Sandiford, 2013), our synthetics show similar waveforms regardless of different CMTZ thickness. This is probably because the Pn wavelength is about 12–16 km at a period of 2 s, thus not able to resolve finer gradient. The dependency of Pn waveforms on source time duration suggests that we need to use smaller earthquakes with shorter duration to constrain the CMTZ. However, small-magnitude earthquakes may not produce waveforms with high SNR. Several previous studies indicate a presence of a low-velocity zone near the base of continental crust (for instance, in Parkfield, California; Ozacar and Zandt, 2009), and a high mantle lie at the uppermost mantle (e.g., Holt and Wallace, 1990; Al-Lazki et al., 2004; Kumar et al., 2007). We further test the cases with negative velocity gradients within the CMTZ featuring low velocity layers at the base of the crust (Fig. S2), and featuring high velocity layers at the uppermost mantle (Fig. S3). The results show that the negative gradients would not lead to a pulse-like Pn, but make Pn more ramp-like (Figs. S2 and S3), which are consistent with the shadow zone effect of the low velocity zone.

Based on a series of forward modeling tests, we observe that Pn waveform changes from step-like to pulse-like due to an increasing thickness of gradient in the CMTZ. In order to quantify the effect of various conditions in CMTZ on Pn shape, we use peak amplitude ratios

of pulse-like Pn to step-like Pn to represent the variation of Pn waveforms (Fig. S4). When the source duration is 0.5 s, a 10 km-thick CMTZ produces 60–70% amplitude variation relative to the jumping velocity case (Fig. S4b). This indicates that Pn amplitude is sensitive to the gradient of the CMTZ.

Another way of quantifying how much the observed Pn waveform looks like a pulse is to define degree of impulsiveness (DOP). We define the DOP as a ratio of peak amplitude in the time window of 1.5 times the source duration after Pn onset to the plateau amplitude which becomes stable about 1 s after the peak (Fig. 3a). For step-like Pn, we observe that the DOP is close to 1.0. As Pn changes to be pulse-like, DOP will increase (Fig. S5). When the source duration is 0.5 s, the DOP for 10 km-thick CMTZ is up to 2.2 which is nearly double of the jumping velocity case (Fig. 3b). In Fig. 3, the lapse time of plateau amplitude is estimated to be 1 s after peak. To investigate the stability of the DOP measurement, we also calculate the ratio of peak amplitude to the plateau amplitude, which arrives 1.0 ± 0.1 s later than the peak, and this peak amplitude only deviates from 5 to 10% of the previous ratio (Fig. S5).

Based on the series of synthetic tests, we find that the Pn waveforms are quite sensitive to the velocity gradient of the CMTZ. We use these results to examine Pn waveforms of regional earthquakes recorded at the permanent stations in east China and South Korea, which are separated by the Yellow Sea, and to constrain the sharpness of the CMTZ. We expect that the similarity of CMTZ to the west and east of Yellow Sea can provide an insight on the tectonic affinity between eastern China and southern Korean Peninsula.

3. Tectonic setting

The tectonic characteristics near and in the vicinity of Yellow Sea have been studied extensively to help understanding the framework of east Asia and tectonic evolution since Paleozoic (e.g., Yin and Nie, 1993; Cheong et al., 2000; Chang and Park, 2001; Sagong et al., 2003; Hao et al., 2007; Kim et al., 2009). To the west of the Yellow Sea, there are two cratons, Sino-Korea Craton and Yangtze Craton, which are separated by a suture zone, Sulu Belt. To the east of Yellow Sea, the Korean

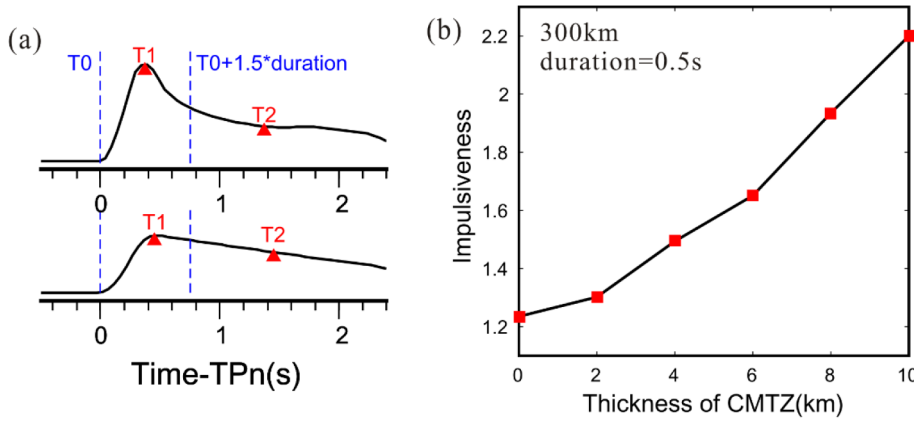


Fig. 3. Degree of impulsiveness of Pn waveforms (Fig. 2b). (a) A schematic cartoon illustrating our approach to quantify the impulsiveness. The impulsiveness is defined as a ratio of peak amplitude (at T1, arrival time of the peak within the time window between the Pn arrival and 1.5 times the source duration) to plateau amplitude (at T2, 1.0 s after T1 arrival). (b) Impulsiveness as a function of thickness of CMTZ for synthetics shown in Fig. 2b.

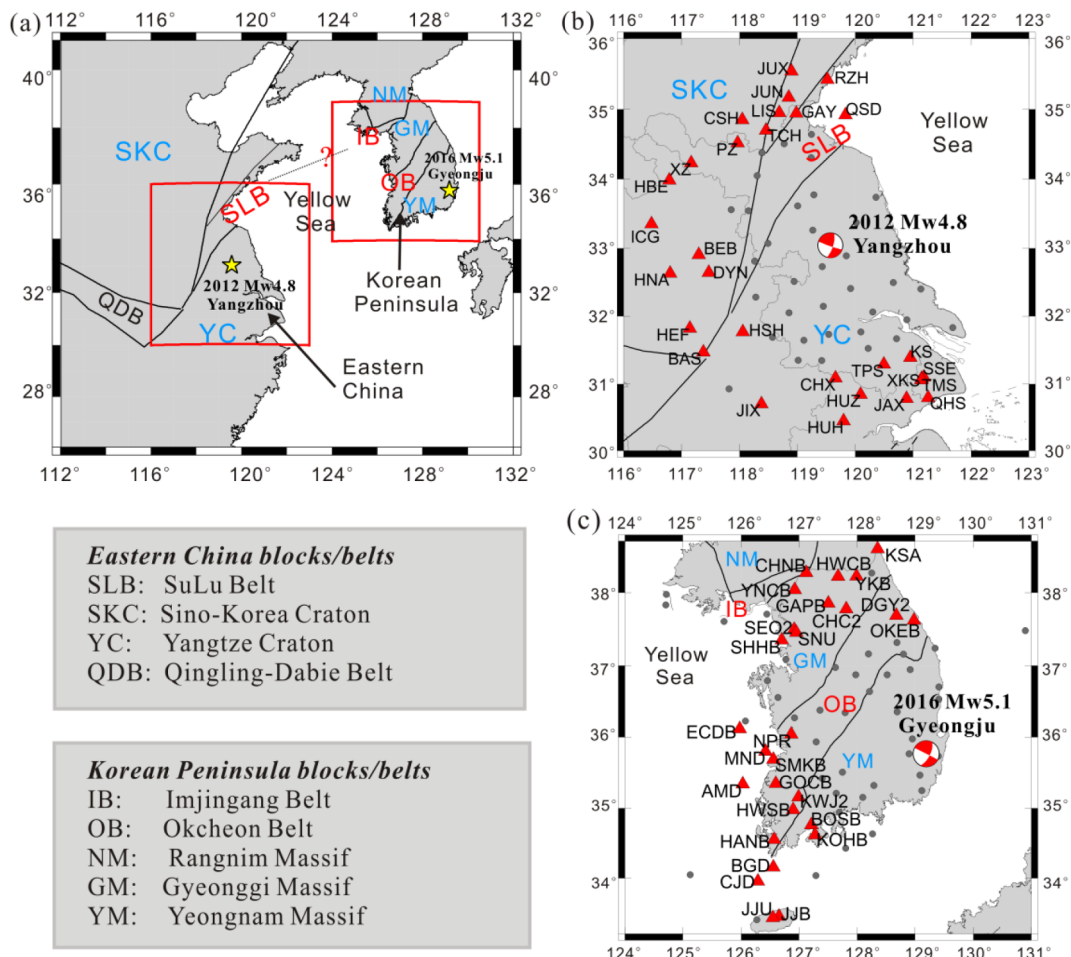


Fig. 4. Maps for tectonic framework, earthquakes and seismic stations. (a) Simplified tectonic map of East Asia. Black solid lines represent tectonic boundaries. The red boxes indicate our study regions, and the yellow stars mark locations of the regional earthquakes used in this study. (b–c) Maps for earthquakes (beachball) and regional stations (triangle). Red triangles indicate stations with clear Pn waveforms. Station codes are displayed near each station. (b) Station distribution and the July 2012 Mw 4.8 Yangzhou event in east China. (c) Station distribution and the September 2016 Mw 5.1 Gyeongju event in South Korea. (For interpretation of the references to colour in this figure legend, the reader is referred to the web version of this article.)

Peninsula is divided into Rangnim Massif, Gyeonggi Massif and Yeongnam Massif by Imjingang Belt and Okcheon Belt from the north to the east (Fig. 4a; Yin and Nie, 1993). The issue of how the Sulu Belt extends to the Peninsula and the tectonic affinity between Korean Peninsula and the eastern China are not yet clear, and thus further studies are needed (e.g., Yin and Nie, 1993; Zhang, 1997; Chang and Park, 2001; Oh et al., 2006; Hao et al., 2007; Zhai et al., 2007; Tang et al., 2010).

Chang and Park (2001) inferred that the Sulu Belt does not extend through the Korean Peninsula as there is lack of evidence such as

ophiolites for such a collision in Korean Peninsula. Hao et al. (2007) demonstrated that there is a nearly north-south fault in the east of Yellow Sea and geophysical features at both sides of the fault are different on the basis of gravity and seismic tomography data. They suggested that the suture zone is located to the west of the Korean Peninsula. In these cases, the Korean Peninsula is a part of the Sino-Korea Craton (Chang and Park, 2001; Hao et al., 2007). However, some studies suggested that the Sulu Belt extended through the Korean Peninsula (Yin and Nie, 1993; Oh et al., 2006; Choi et al., 2006; Chang and Baag,

2012 Mw 4.8 Yangzhou earthquake

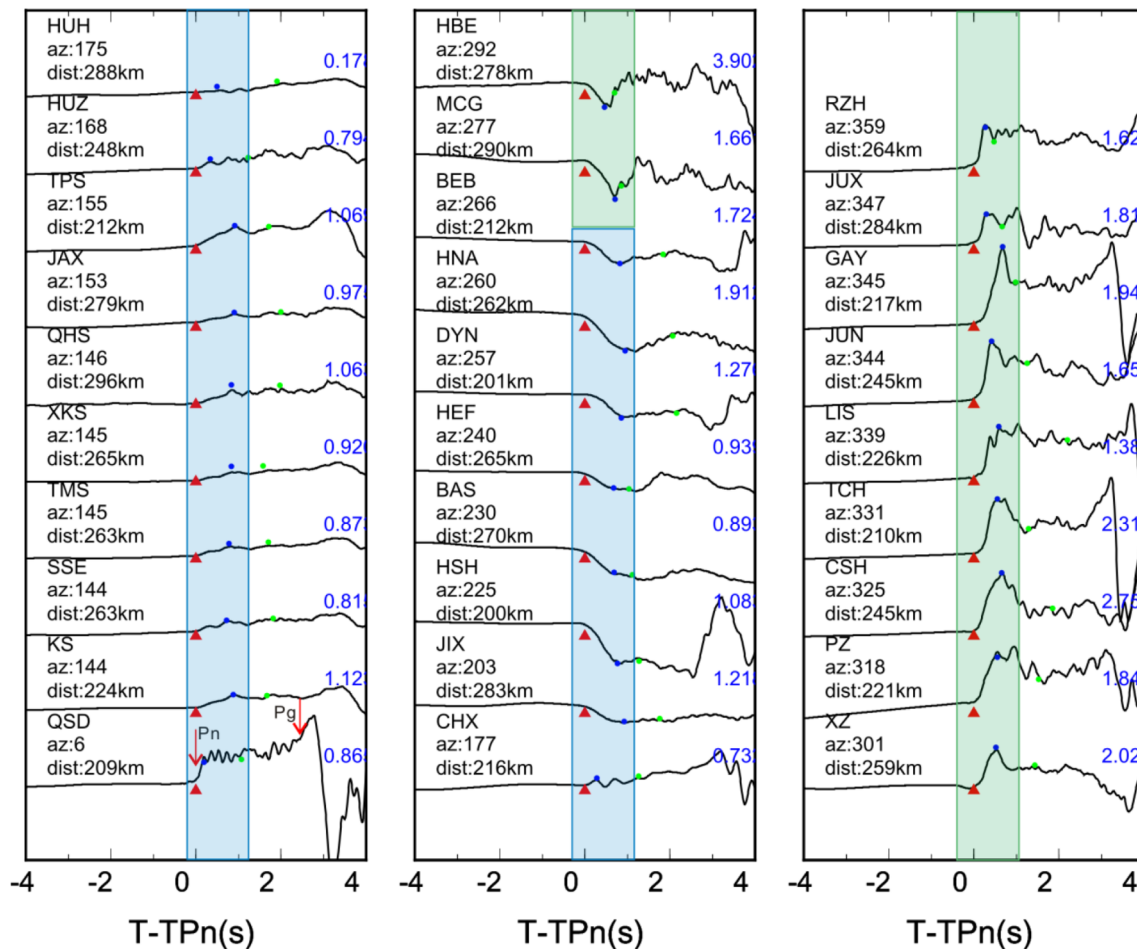


Fig. 5. Vertical-component displacement waveform for Yangzhou earthquake (Fig. 4b). Each waveform is aligned on the picked first break of Pn (red triangle) whose arrival time is at least 1 s earlier than the Pg (red arrows). Pn waveforms are also framed by shadows to make them distinguished easily. The seismograms are sorted with station azimuth. Station code, azimuth (az; in degree) and epicentral distance (dist) are displayed at the upper left of each trace. The numbers in blue indicate impulsiveness, defined as a ratio of the peak amplitude (blue dot) to the plateau amplitude (green dot). Arrivals for Pn and Pg are highlighted as red arrows. (For interpretation of the references to colour in this figure legend, the reader is referred to the web version of this article.)

2007). Yin and Nie (1993) suspected that the occurrence of ophiolites is not a necessary condition for the collision hypothesis, and suggested that Sulu Belt is connected with the Imjingang Belt as the strata of Gyeonggi Massif is similar to Sino-Korea Craton, based on geological chronology and distribution of rocks and strata in eastern China and southern Korea. A presence of eclogite in the southwestern Gyeonggi Massif and mangerites in Odesan area of the eastern Gyeonggi Massif further support that Sulu Belt may extend into Korean Peninsula (Oh et al., 2006). Choi et al. (2006) inferred that the Sulu Belt extends in an ENE direction to the region near Imjingang Belt in the western Korean Peninsula based on the gravity data. In this case, the Korean Peninsula is divided into two parts such that the north belongs to the Sino-Korea Craton while the south belongs to the Yangtze Craton (Choi et al., 2006). This model is consistent with previous studies that conclude that the Okcheon Belt is not a collision zone and Gyeonggi Massif and Yeongnam Massif have similar crustal evolution history (Cluzel, 1992; Chang, 1996; Lee et al., 1998; Cheong et al., 2000, 2003).

4. Data and results

In this study, we choose earthquakes with magnitudes between 4.0 and 5.5. As we demonstrated from the synthetic tests in the previous section, events smaller than magnitude 5.5 ensure short source

durations and simple source time functions. In addition, events larger than magnitude 4.0 produce clear Pn. For a shallow earthquake, a depth phase may contaminate Pn waveforms (Ma, 2010), and this will be discussed in the next section. In order to keep Pn isolated from any subsequent depth phase, relatively deep earthquakes are chosen. Recently, several moderately strong earthquakes have occurred in our study region, including the July 2012 Mw 4.8 Yangzhou earthquake in eastern China (Hong et al., 2013) and the September 2016 Mw 5.1 Gyeongju earthquake in southern Korea (Kim et al., 2016, 2017). This Mw 5.1 is a foreshock of the Mw 5.5 event (Kim et al., 2016, 2017). Waveforms of these two earthquakes were well recorded by regional networks in China (Zheng et al., 2010) and South Korea (Fig. 4b and c). Stations with epicentral distance between 200 km and 500 km are chosen to make sure Pn is clear and arrives earlier than Pg (Figs. 5 and 6). We reject the stations with low SNR for Pn, which are located at coast or near the nodal plane of P wave.

The waveforms are aligned on the hand-picked Pn arrivals (Figs. 5 and 6, red triangle), and arranged in azimuth to examine azimuth dependency on the waveform. For the Yangzhou earthquake, there are obvious azimuthal variations in Pn waveforms. The recorded Pn waveforms from the stations in the south of the earthquake source are step-like whereas the northern stations are pulse-like (Fig. 5). Based on our forward modeling results, this observed difference implies that the

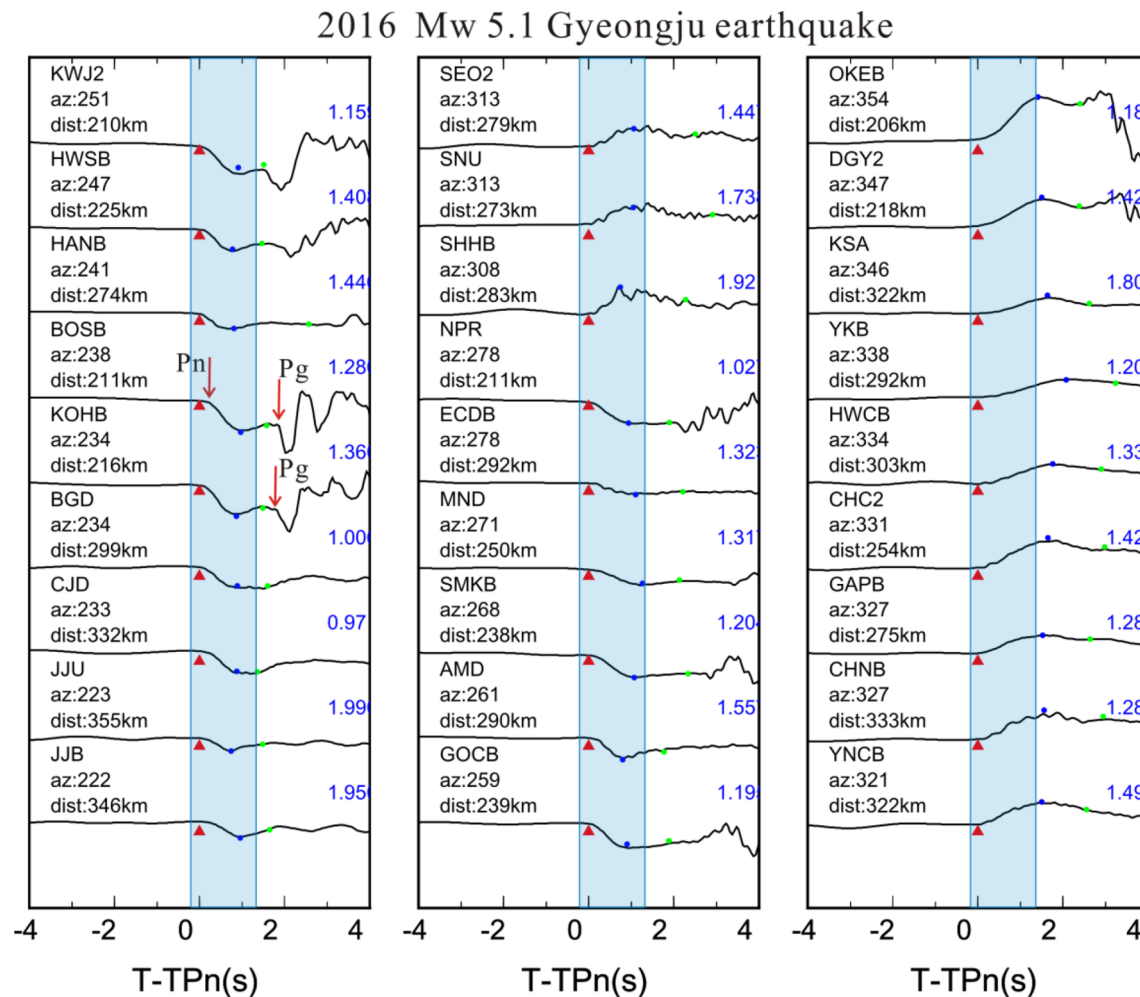


Fig. 6. Vertical-component displacement waveform for Gyeongju earthquake (Fig. 4c). See a caption of Fig. 5 for texts and symbols drawn in the figure.

CMTZ in the south of the Yangtze Craton is sharp while there may be thick gradient CMTZ in the north. For the Gyeongju earthquake, the Pn waveforms mostly show step-like shapes, and this feature is coherent in different azimuth (Fig. 6). This observation suggests that the Moho in this region is sharp, suggesting that southern Korean Peninsula is underlain by sharp CMTZ.

We calculate the ratio of peak amplitude to plateau amplitude to quantify the DOP of the observed records. Arrival times for both the peak amplitude and the plateau amplitude are picked manually as the waveforms after Pn peak are not as smooth as in the synthetics, which could be caused by small-scale three-dimensional effects (Figs. 5 and 6). For the observed step-like records, the DOP is usually less than 1.5 while DOP is up to 2.0 or even higher for the pulse-like Pn. Some anomalous DOP are also observed as the stations may be near the nodal plane of P wave.

We note that our method of resolving CMTZ structure with Pn waveform data may fail when the earthquake focal depth is shallow. For example, the observed Pn waveforms of the November 2017 Mw 5.4 Pohang earthquake in South Korea do not show the step-like characteristics of the CMTZ (solid lines in Fig. 7). We suspect that the Pn waveforms are contaminated by the subsequent depth phase sPn due to its shallow depth (5 km determined by SLUEC, Saint Louis University Earthquake Center). This depth estimate is also consistent with recent studies (Grigoli et al., 2018; Kim et al., 2018). To understand whether the observation of abnormal Pn from 2017 Mw 5.4 Pohang earthquake is related to the shallow epicenter depth, we calculate synthetic seismograms for two focal depths as 5 km and 10 km (Fig. 7). The focal

mechanism from SLUEC (NP1:231°/72°/154°, NP2:330°/65°/20°) is similar to that of Global Centroid Moment Tensor (NP1:231°/77°/151°, NP2:327°/66°/14°). The simplified velocity model (Fig. 1b) is used to reduce the interference of the seismic multiples from crustal interfaces. The synthetics show that Pn is step-like when the focal depth is 10 km (dotted lines in Fig. 7) while the step is smeared for the shallower case (dashed lines in Fig. 7), as the observed data. We calculate the theoretical travel time of sPn, and mark sPn on the synthetic waveforms (arrows in Fig. 7). The small travel time difference between sPn and Pn for shallow earthquake demonstrates that Pn is contaminated by sPn. The similarity between the observed data and synthetic data with the 5 km focal depth implies that the Pohang earthquake is indeed shallow as suggested by previous studies (Grigoli et al., 2018; Kim et al., 2018). This result suggests that a relatively deep earthquake is preferable for modeling Pn waveform to constrain the CMTZ structure.

5. Discussion

In addition to the velocity gradient in CMTZ, the topography of CMTZ may also cause changes in Pn waveforms. The CMTZ in this study area of eastern China is relatively flat with the topography no more than 2 km relative to the average Moho depth (Zhang et al., 2011). Therefore, the pulse-like Pn in the north of the Yangtze Plate would be more probably caused by positive gradient CMTZ. The DOP from most records in the north of Yangtze Craton is 1.6–2.0. According to impulsiveness measurement (Fig. 3), this would suggest 6–10 km thick CMTZ if we take the duration of this Mw 4.8 earthquake as 0.5 s

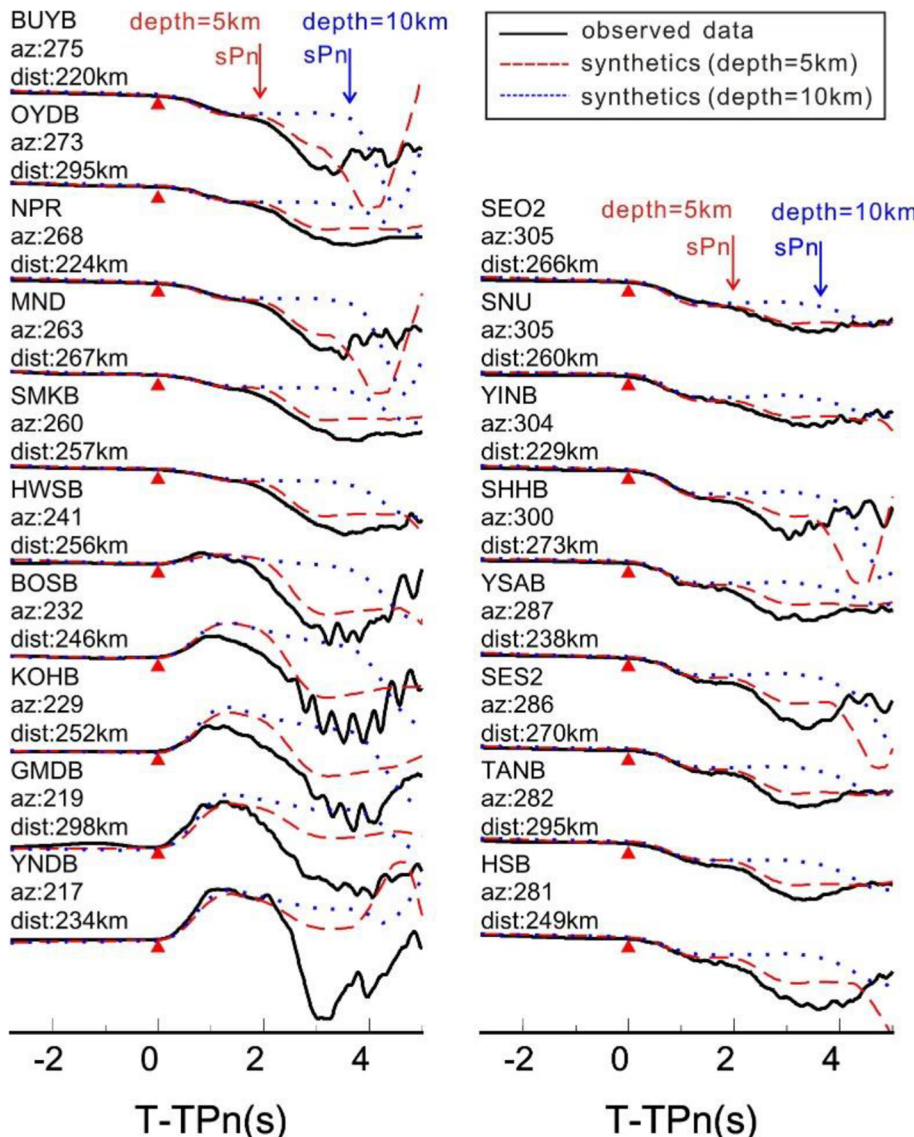


Fig. 7. Vertical-component displacement waveforms of observed data (black solid line) and synthetics (red dashed line and blue dotted line for focal depth of 5 km and 10 km, respectively) for November 2017 Mw 5.4 Pohang earthquake in South Korea. See Fig. S6 for the earthquake location in a map view. The waveforms are aligned on Pn first break (red triangle). The theoretical times of sPn are marked with red and blue arrows for the synthetics with the depths of 5 km and 10 km, respectively. The seismograms are sorted with station azimuth. Station code, azimuth (az; in degree) and epicentral distance (dist) are displayed at the upper left of each trace. (For interpretation of the references to colour in this figure legend, the reader is referred to the web version of this article.)

(Fig. 3). Previous studies (Zhang et al., 2000; Lin and Wang, 2005; Zheng et al., 2006) also support our observation. For example, Zheng et al. (2006) suggested a 5–10 km thick CMTZ in North China Craton via joint study of receiver functions, waveform inversion and gravity modeling. Lin and Wang (2005) summarized the CMTZ styles of China from seismic profiles, which showed that there might be a relatively thick CMTZ (2–5 km) in North China Craton while the CMTZ in South China is sharp with a thickness of 2–3 km. These studies are consistent with the observation of Pn waveforms at different azimuth for Yangzhou earthquake (Fig. 5). However, for other regions with substantial Moho topography, methods for calculating accurate synthetics for complicated models are needed, such as FD and SEM (Komatitsch and Tromp, 1999; Zhang et al., 2014).

In this study, the consistent step-like Pn (Fig. 6) implies that the CMTZ beneath the southern Korean Peninsula is sharp with its thickness less than 2 km. The sharp Moho in Korea is supported by receiver functions studies as we can see clear first reflections, such as Ppss and Ppss, which only can be seen if the CMTZ is sharp (Chang et al., 2004; Yoo et al., 2007). In southern part of Korea Peninsular, the shallow crust features obvious lateral variation manifested by orogens and basins. But the deep crust seems to be relatively simple as demonstrated with the step-like Pn waveforms. The different features of the shallow and deep crust might imply distinct evolution history. Comparing

characteristics of Pn waveforms from the two earthquakes, we find that the CMTZ beneath the southern Korean Peninsula is more similar to the south of the Yangtze Craton than the north (Figs. 5 and 6). The similarity in the observed seismic waveforms suggests that the extension line of the Sulu Belt may be to the north of the Gyeonggi Massif. The result is similar to a research based on H-K method (Zhu and Kanamori, 2000) with receiver function (Langston, 1979) that P-to-S velocity ratio (V_p/V_s) in southern Korean Peninsula is closed to Yangtze Craton (Chang and Baag, 2007). We also notice that the V_p/V_s near Gyeongju earthquake is slightly higher than the northwest (Chang and Baag, 2007), which cannot be recovered by Pn as the ray path of Pn does not sample the CMTZ near source.

We observe step-like Pn in Yangtze Craton and pulse-like Pn in the Sino-Korea Craton. The observation of Pn in southern Korean Peninsula is step-like suggesting the CMTZ in southern Korean Peninsula is similar to Yangtze Craton. Since pulse-like Pn is not observed in southern Korean Peninsula, stations to the north of our study area (Fig. 4) and ocean-bottom seismometers in the Yellow Sea are preferred to resolve whether the Sulu Belt extends along the north of the Gyeonggi Massif or the eastern edge of the Yellow Sea. However, the physical mechanism of generating gradient CMTZ is not yet clear. Pressure, temperature, metamorphism and the petrologic transition from olivine-poor to olivine-rich compositions might have significant influence on seismic

properties of lower crustal and mantle rocks (Wang et al., 2013a, 2013b; Thybo et al., 2013). Thus, further tectonic and petrologic researches are required to provide additional constraints on gradient velocity structures.

However, Pn waveform data only provide partial constraints on CMTZ mainly due to its propagation in the horizontal direction along the Moho. Our Pn analysis together with receiver functions (near-vertical rays) can resolve detailed CMTZ structure.

6. Conclusions

In this study, we first demonstrate from the synthetic tests that Pn waveforms are effective to constrain the velocity structure of crust-mantle transition zone (CMTZ). Thickened positive gradient CMTZ leads to the change of Pn shape from step-like to pulse-like. The amplitude ratio between pulse-like waveform and step-like waveform can assess the variation of the Pn shape. For a source duration of 0.5 s, 10 km-thick CMTZ generates 60% variation of the amplitude as compared to the sharp Moho case. Furthermore, the amplitude ratio of peak to plateau can quantify the degree of impulsiveness (DOP). For the step-like waveform, the DOP is usually less than 1.5 while DOP is up to 2 or even higher for the pulse-like Pn.

We then use moderate-size earthquakes in eastern China (Yangzhou earthquake) and southern Korea (Gyeongju earthquake) as examples to constrain the CMTZ structures surrounding the Yellow Sea. To the west of Yellow Sea, CMTZ in the south of Yangtze Craton is sharp while there may be a positive gradient CMTZ with 6–10 km thickness in the north. To the east of Yellow Sea, CMTZ beneath the Korean Peninsula is sharp which is similar to the south of Yangtze Craton. The similarity in the Pn waveforms indicates the Sulu Belt may extend along the north of the Gyeonggi Massif which is consistent with previous studies based on geological chronology and receiver functions (Yin and Nie, 1993; Chang and Baag, 2007).

7. Data and resources

The data of Yangzhou earthquake for this study are provided by Data Management Centre of China National Seismic Network at Institute of Geophysics (SEISDMC, doi: <https://doi.org/10.11998/SeisDmc/SN>). The data of Gyeongju and Pohang earthquakes are from the Korea Institute of Geoscience and Mineral Resources (KIGAM) and the Korea Meteorological Administration (KMA) which are available with permissions at <http://quake.kigam.re.kr> and <http://necis.kma.go.kr>, respectively. Moment tensor solutions were obtained from the Global Centroid Moment Tensor Catalog (<https://www.globalcmt.org/CMTsearch.html>) and from the Saint Louis University Earthquake Center (http://www.eas.slu.edu/eqc/eqc_mt/MECH.KR).

Acknowledgments

We thank the SEISDMC, KMA and KIGAM for providing seismic-waveform data. Seismic Analysis Code (SAC) and Generic Mapping Tools (GMT) code (Wessel and Smith, 1998) are used for data processing and figure plotting. This study is supported by funding from the Strategic Priority Research Program (B) of Chinese Academy of Sciences (grant XDB18000000), National Basic Research Program of China (973 Program, 2014CB845901) and Natural Science Foundation of China (41874068). Y. Kim acknowledges Creative-Pioneering Researchers Program through Seoul National University (SNU SRnD 3345-20160014). We also thank the editor Vernon Cormier, and two reviewers for their insightful and thoughtful comments to improve this manuscript.

Appendix A. Supplementary material

Supplementary data to this article can be found online at <https://doi.org/10.1016/j.pepi.2019.01.008>.

References

- Abbott, D.H., Mooney, W.D., VanTongeren, J.A., 2013. The character of the Moho and lower crust within Archean cratons and the tectonic implications. *Tectonophysics* 609, 690–705.
- Aki, K., Richards, P.G., 2002. Quantitative Seismology. University Science Books, Sausalito, California.
- Al-Lazki, A.I., Sandvol, E., Seber, D., Barazangi, M., Turkelli, N., Mohamad, R., 2004. Pn tomographic imaging of mantle lid velocity and anisotropy at the junction of the Arabian, Eurasian and African plates. *Geophys. J. Int.* 158 (3), 1024–1040.
- Braile, L.W., Smith, R.B., 1975. Guide to the interpretation of crustal refraction profiles. *Geophys. J. R. Astron. Soc.* 40 (2), 145–176.
- Brun, J.P., Gutscher, M.A., 1992. Deep crustal structure of the Rhine Graben from DEKORP-ECORS seismic reflection data: a summary. *Tectonophysics* 208 (1–3), 139–147.
- Buehler, J.S., Shearer, P.M., 2017. Uppermost mantle seismic velocity structure beneath USArray. *J. Geophys. Res. Solid Earth* 122 (1), 436–448.
- Carbonell, R., Gallart, J., Perez-Estaun, A., 2002. Modelling and imaging the Moho transition: the case of the southern Urals. *Geophys. J. Int.* 149 (1), 134–148.
- Carbonell, R., Levander, A., Kind, R., 2013. The Mohorovičić discontinuity beneath the continental crust: An overview of seismic constraints. *Tectonophysics* 609, 353–376.
- Chapman, C.H., 1978. A new method for computing synthetic seismograms. *Geophys. J. R. Astron. Soc.* 54 (3), 481–518.
- Chang, E.Z., 1996. Collisional orogeny between north and south China and its eastern extension in the Korean Peninsula. *J. SE Asian Earth Sci.* 13 (3–5), 267–277.
- Chang, K.H., Park, S.O., 2001. Paleozoic Yellow Sea Transform Fault: its role in the tectonic history of Korea and adjacent regions. *Gondwana Res.* 4 (4), 588–589.
- Chang, S.J., Baag, C.E., Langston, G.A., 2004. Joint analysis of teleseismic receiver functions and surface wave dispersion using the genetic algorithm. *Bull. Seismol. Soc. Am.* 94 (2), 691–704.
- Chang, S.J., Baag, C.E., 2007. Moho depth and crustal Vp/Vs variation in southern Korea from teleseismic receiver functions: implication for tectonic affinity between the Korean Peninsula and China. *Bull. Seismol. Soc. Am.* 97 (5), 1621–1631.
- Cheong, C.S., Kwon, S.T., Park, K.H., 2000. Pb and Nd isotopic constraints on Paleoproterozoic crustal evolution of the northeastern Yeongnam massif, South Korea. *Precambrian Res.* 102 (3), 207–220.
- Cheong, C.S., Jeong, G.Y., Kim, H., Choi, M.S., Lee, S.H., Cho, M., 2003. Early Permian peak metamorphism recorded in U-Pb system of black slates from the Ogcheon metamorphic belt, South Korea, and its tectonic implication. *Chem. Geol.* 193 (1–2), 81–92.
- Choi, S., Oh, C.W., Luehr, H., 2006. Tectonic relation between northeastern China and the Korean peninsula revealed by interpretation of GRACE satellite gravity data. *Gondwana Res.* 9 (1–2), 62–67.
- Cluzel, D., 1992. Ordovician bimodal magmatism in the Ogcheon belt (South Korea): intracontinental rift-related volcanic activity. *J. SE Asian Earth Sci.* 7 (2–3), 195–209.
- Cook, F.A., 2002. Fine structure of the continental refraction Moho. *Bull. Geol. Soc. Am.* 114 (1), 64–79.
- Di Stefano, R., Chiarabba, C., Lucente, F., Amato, A., 1999. Crustal and uppermost mantle structure in Italy from the inversion of P-wave arrival times: Geodynamic implications. *Geophys. J. Int.* 139 (2), 483–498.
- Flecha, I., Palomeras, I., Carbonell, R., Simancas, F., Ayarza, P., Matas, J., et al., 2009. Seismic imaging and modelling of the lithosphere of SW-Iberia. *Tectonophysics* 472 (1–4), 148–157.
- Gao, R., Huang, D., Lu, D., Qian, G., Li, Y., Kuang, C., et al., 2000. Deep seismic reflection profile across the juncture zone between the Tarim Basin and the West Kunlun Mountains. *Chin. Sci. Bull.* 45 (24), 2281.
- Gibson, G., Sandiford, M., 2013. Seismicity and induced earthquakes. Office of the New South Wales Chief Scientist and Engineer.
- Grigoli, F., Cesca, S., Rinaldi, A.P., Manconi, A., López-Comino, J.A., Clinton, J.F., et al., 2018. The November 2017 Mw 5.5 Pohang earthquake: A possible case of induced seismicity in South Korea. *Science* 360 (6392), 1003–1006.
- Hale, L.D., Thompson, G.A., 1982. The seismic reflection character of the continental Mohorovičić discontinuity. *J. Geophys. Res. Solid Earth* 87 (B6), 4625–4635.
- Hao, T.Y., Xu, Y., Suh, M., Liu, J.H., Zhang, L.L., Dai, M.G., 2007. East Marginal Fault of the Yellow Sea: a part of the conjunction zone between Sino-Korea and Yangtze Blocks? *Geol. Soc., London, Spec. Publ.* 280 (1), 281–291.
- Hawkesworth, C., Cawood, P., Dhuime, B., 2013. Continental growth and the crustal record. *Tectonophysics* 609, 651–660.
- Hearn, T.M., Wang, S., Ni, J.F., Xu, Z., Yu, Y., Zhang, X., 2004. Uppermost mantle velocities beneath China and surrounding regions. *J. Geophys. Res. Solid Earth* 109 (B11).
- Helmbberger, D.V., 1968. The crust-mantle transition in the Bering Sea. *Bull. Seismol. Soc. Am.* 58 (1), 179–214.
- Hole, J.A., 1992. Nonlinear high-resolution three-dimensional seismic travel time tomography. *J. Geophys. Res. Solid Earth* 97 (B5), 6553–6562.
- Holt, W.E., Wallace, T.C., 1990. Crustal thickness and upper mantle velocities in the Tibetan Plateau region from the inversion of regional Pn waveforms: Evidence for a thick upper mantle lid beneath southern Tibet. *J. Geophys. Res. Solid Earth* 95 (B8), 12499–12525.
- Hong, D.Q., Wang, X.Z., Ni, H.Y., Li, F., 2013. Focal mechanism and focal depth of July 20, 2012 Jiangsu Gaoyou M 4.9 earthquake. *Prog. Geophys.* 28 (4), 1757–1765.
- Hong, T.K., Choi, H., 2012. Seismological constraints on the collision belt between the North and South China blocks in the Yellow Sea. *Tectonophysics* 570, 102–113.
- Kim, K.H., Ree, J.H., Kim, Y., Kim, S., Kang, S.Y., Seo, W., 2018. Assessing whether the 2017 Mw 5.4 Pohang earthquake in South Korea was an induced event. *Science*

- eaat6081.
- Kim, S.W., Kwon, S., Ryu, I.C., 2009. Geochronological constraints on multiple deformations of the Honam Shear Zone, South Korea and its tectonic implication. *Gondwana Res.* 16 (1), 82–89.
- Kim, Y., Rhee, J., Kang, T.-S., Kim, K.-H., Kim, M., Lee, S.-J., 2016. The 12 September 2016 Gyeongju earthquakes: 1. Observation and remaining questions. *Geosci. J.* 20 (6), 747–752. <https://doi.org/10.1007/s12303-016-0033-x>.
- Kim, Y., He, X., Ni, S., Lim, H., Park, S.C., 2017. Earthquake source mechanism and rupture directivity of the 12 September 2016 M w 5.5 Gyeongju, South Korea, Earthquake. *Bull. Seismological Soc. Am.* 107 (5), 2525–2531.
- Komatitsch, D., Tromp, J., 1999. Introduction to the spectral element method for three-dimensional seismic wave propagation. *Geophys. J. Int.* 139 (3), 806–822.
- Kumar, P., Yuan, X., Kumar, M.R., Kind, R., Li, X., Chadha, R.K., 2007. The rapid drift of the Indian tectonic plate. *Nature* 449 (7164), 894.
- Langston, C.A., 1979. Structure under Mount Rainier, Washington, inferred from teleseismic body waves. *J. Geophys. Res. Solid Earth* 84 (B9), 4749–4762.
- Lee, K.S., Chang, H.W., Park, K.H., 1998. Neoproterozoic bimodal volcanism in the central Ognecheon belt, Korea: age and tectonic implication. *Precambr. Res.* 89 (1–2), 47–57.
- Liang, C., Song, X., Huang, J., 2004. Tomographic inversion of Pn travel times in China. *J. Geophys. Res. Solid Earth* 109 (B11).
- Lin, G., Wang, Y., 2005. The P-wave velocity structure of the crust–mantle transition zone in the continent of China. *J. Geophys. Eng.* 2 (3), 268.
- Li, D., Helmberger, D., Clayton, R.W., Sun, D., 2014. Global synthetic seismograms using a 2-D finite-difference method. *Geophys. J. Int.* 197 (2), 1166–1183.
- Li, Z., Xu, Y., Hao, T., Liu, J., Zhang, L., 2006. Seismic tomography and velocity structure in the crust and upper mantle around Bohai Sea area. *Chin. J. Geophys.* 49 (3), 698–706.
- Li, Z., Ni, S., Hao, T., Xu, Y., Roecker, S., 2012. Uppermost mantle structure of the eastern margin of the Tibetan plateau from interstation Pn traveltimes difference tomography. *Earth Planet. Sci. Lett.* 335, 195–205.
- Ma, S., 2010. Focal depth determination for moderate and small earthquakes by modeling regional depth phases sPg, sPmP, and sPn. *Bull. Seismol. Soc. Am.* 100 (3), 1073–1088.
- Mengel, K., Kern, H., 1992. Evolution of the petrological and seismic Moho-implications for the continental crust-mantle boundary. *Terra Nova* 4 (1), 109–116.
- Mjelde, R., Goncharov, A., Müller, R.D., 2013. The Moho: boundary above upper mantle peridotites or lower crustal eclogites? A global review and new interpretations for passive margins. *Tectonophysics* 609, 636–650.
- Morozov, I.B., Smithson, S.B., Chen, J., Hollister, L.S., 2001. Generation of new continental crust and terrane accretion in southeastern Alaska and western British Columbia: Constraints from P- and S-wave wide-angle seismic data (ACCRETE). *Tectonophysics* 341 (1–4), 49–67.
- Myers, S.C., Begnaud, M.L., Ballard, S., Pasynnos, M.E., Phillips, W.S., Ramirez, A.L., et al., 2010. A crust and upper-mantle model of Eurasia and North Africa for Pn travel-time calculation. *Bull. Seismol. Soc. Am.* 100 (2), 640–656.
- Niu, F., James, D.E., 2002. Fine structure of the lowermost crust beneath the Kaapvaal craton and its implications for crustal formation and evolution. *Earth Planet. Sci. Lett.* 200 (1), 121–130.
- Oh, C.W., Krishnan, S., Kim, S.W., Kwon, Y.W., 2006. Mangerite magmatism associated with a probable Late-Permian to Triassic Hongseong-Odesan collision belt in South Korea. *Gondwana Res.* 9 (1–2), 95–105.
- O'Reilly, S.Y., Griffin, W.L., 2013. Moho vs crust–mantle boundary: evolution of an idea. *Tectonophysics* 609, 535–546.
- Owens, T.J., Zandt, G., 1985. The response of the continental crust–mantle boundary observed on broadband teleseismic receiver functions. *Geophys. Res. Lett.* 12 (10), 705–708.
- Owens, T.J., Zandt, G., 1997. Implications of crustal property variations for models of Tibetan plateau evolution. *Nature* 387 (6628), 37.
- Ozacar, A.A., Zandt, G., 2009. Crustal structure and seismic anisotropy near the San Andreas Fault at Parkfield, California. *Geophys. J. Int.* 178 (2), 1098–1104.
- Palomeras, I., Carbonell, R., Flecha, I., Simancas, F., Ayarza, P., Matas, J., et al., 2009. Nature of the lithosphere across the Variscan orogen of SW Iberia: Dense wide-angle seismic reflection data. *J. Geophys. Res. Solid Earth* 114 (B2).
- Palomeras, I., Carbonell, R., Ayarza, P., Martí, D., Brown, D., Simancas, J.F., 2011. Shear wave modeling and Poisson's ratio in the Variscan Belt of SW Iberia. *Geochem., Geophys., Geosyst.* 12 (7).
- Pei, S., Zhao, J., Sun, Y., Xu, Z., Wang, S., Liu, H., Gao, X., 2007. Upper mantle seismic velocities and anisotropy in China determined through Pn and Sn tomography. *J. Geophys. Res. Solid Earth* 112 (B5).
- Prodehl, C., 1977. The structure of the crust–mantle boundary beneath North America and Europe as derived from explosion seismology. *The Earth's Crust* 349–369.
- Prodehl, C., Mooney, W.D. (Eds.), 2012. Exploring the Earth's crust: history and results of controlled-source seismology. Geological Society of America.
- Sagong, H., Cheong, C.S., Kwon, S.T., 2003. Paleoproterozoic orogeny in South Korea: evidence from Sm–Nd and Pb step-leaching garnet ages of Precambrian basement rocks. *Precambr. Res.* 122 (1–4), 275–295.
- Savage, B., Ji, C., Helmberger, D.V., 2003. Velocity variations in the uppermost mantle beneath the southern Sierra Nevada and Walker Lane. *J. Geophys. Res. Solid Earth* 108 (B7).
- Scholz, C.H., 1998. Earthquakes and friction laws. *Nature* 391 (6662), 37.
- Sun, W., Kennett, B.L.N., 2016. Uppermost mantle structure beneath eastern China and its surroundings from Pn and Sn tomography. *Geophys. Res. Lett.* 43 (7), 3143–3149.
- Tang, X.J., Yu, W.H., Shan, R., 2010. The mesozoic plate boundary in the Eastern China and Korean Peninsula: Present studies and problems. *Acta Geologica Sinica* 84 (5), 606–617.
- Tian, X., Zelt, C.A., Wang, F., Jia, S., Liu, Q., 2014. Crust structure of the North China Craton from a long-range seismic wide-angle-reflection/refraction data. *Tectonophysics* 634, 237–245.
- Tian, Y., Zhao, D., Sun, R., Teng, J., 2009. Seismic imaging of the crust and upper mantle beneath the North China Craton. *Phys. Earth Planet. Inter.* 172 (3–4), 169–182.
- Teng, J., Zhang, Z., Zhang, X., Wang, C., Gao, R., Yang, B., et al., 2013. Investigation of the Moho discontinuity beneath the Chinese mainland using deep seismic sounding profiles. *Tectonophysics* 609, 202–216.
- Thybo, H., Artemieva, I.M., 2013. Moho and magmatic underplating in continental lithosphere. *Tectonophysics* 609, 605–619.
- Thybo, H., Artemieva, I.M., Kennett, B., 2013. Moho: 100years after Andrija Mohorovičić. *Tectonophysics* 609, 1–8.
- Uhlmann, G., 2001. Travel time tomography. *J. Korean Math. Soc.* 38 (4), 711–722.
- Vidale, J.E., Helmberger, D.V., 1988. Elastic finite-difference modeling of the 1971 San Fernando, California earthquake. *Bull. Seismol. Soc. Am.* 78 (1), 122–141.
- Wang, Q., Bagdassarov, N., Ji, S., 2013a. The Moho as a transition zone: A revisit from seismic and electrical properties of minerals and rocks. *Tectonophysics* 609, 395–422.
- Wang, R., 1999. A simple orthonormalization method for stable and efficient computation of Green's functions. *Bull. Seismol. Soc. Am.* 89 (3), 733–741.
- Wang, S., Niu, F., Zhang, G., 2013b. Velocity structure of the uppermost mantle beneath East Asia from Pn tomography and its dynamic implications. *J. Geophys. Res. Solid Earth* 118 (1), 290–301.
- Wessel, P., Smith, W.H., 1998. New, improved version of generic mapping tools released. *Eos, Trans. Am. Geophys. Union* 79 (47), 579.
- Xie, X.B., Lay, T., 2016. Frequency-dependent effects of 2D random velocity heterogeneities in the mantle lid on Pn geometric spreading. *Bull. Seismol. Soc. Am.* 107 (1), 482–488.
- Xu, Y., Liu, F., Liu, J., Chen, H., 2002. Crust and upper mantle structure beneath western China from P wave travel time tomography. *J. Geophys. Res.: Solid Earth* 107 (B10), ESE-4.
- Yang, X., Lay, T., Xie, X.B., Thorne, M.S., 2007. Geometric spreading of Pn and Sn in a spherical Earth model. *Bull. Seismol. Soc. Am.* 97 (6), 2053–2065.
- Yao, Z.X., Harkrider, D.G., 1983. A generalized reflection-transmission coefficient matrix and discrete wavenumber method for synthetic seismograms. *Bull. Seismol. Soc. Am.* 73 (6A), 1685–1699.
- Yin, A., Nie, S., 1993. An indentation model for the North and South China collision and the development of the Tan-Lu and Honam fault systems, eastern Asia. *Tectonics* 12 (4), 801–813.
- Yoo, H.J., Herrmann, R.B., Cho, K.H., Lee, K., 2007. Imaging the three-dimensional crust of the Korean Peninsula by joint inversion of surface-wave dispersion and teleseismic receiver functions. *Bull. Seismol. Soc. Am.* 97 (3), 1002–1011.
- Zhai, M.G., Guo, J.H., Li, Z., Chen, D.Z., Peng, P., Li, T.S., Hu, B., 2007. Extension of the Sulu UHP belt to the Korean Peninsula: evidence from orogenic belts, Precambrian basements and Paleozoic sedimentary basins. *Geol. J. China Univ.* 13 (3), 415–428.
- Zhang, K.J., 1997. North and South China collision along the eastern and southern North China margins. *Tectonophysics* 270 (1), 145–156.
- Zhang, W., Zhang, Z., Chen, X., 2012. Three-dimensional elastic wave numerical modelling in the presence of surface topography by a collocated-grid finite-difference method on curvilinear grids. *Geophys. J. Int.* 190 (1), 358–378.
- Zhang, Z., Li, Y., Lu, D., Teng, J., Wang, G., 2000. Velocity and anisotropy structure of the crust in the Dabieshan orogenic belt from wide-angle seismic data. *Phys. Earth Planet. Inter.* 122 (1–2), 115–131.
- Zhang, Z., Yang, L., Teng, J., Badal, J., 2011. An overview of the earth crust under China. *Earth Sci. Rev.* 104 (1–3), 143–166.
- Zhang, Z., Zhang, W., Chen, X., 2014. Three-dimensional curved grid finite-difference modelling for non-planar rupture dynamics. *Geophys. J. Int.* 199 (2), 860–879.
- Zheng, T., Chen, L., Zhao, L., et al., 2006. Crust–mantle structure difference across the gravity gradient zone in North China Craton: seismic image of the thinned continental crust. *Phys. Earth Planet. Inter.* 159 (1), 43–58.
- Zheng, T.Y., Zhao, L., Zhu, R.X., 2008. Insight into the geodynamics of cratonic reactivation from seismic analysis of the crust–mantle boundary. *Geophys. Res. Lett.* 35 (8).
- Zheng, X.F., Yao, Z.X., Liang, J.H., Zheng, J., 2010. The role played and opportunities provided by IGP DMC of China National Seismic Network in Wenchuan earthquake disaster relief and researches. *Bull. Seismol. Soc. Am.* 100, 2866–2872.
- Zhu, L., Kanamori, H., 2000. Moho depth variation in southern California from teleseismic receiver functions. *J. Geophys. Res. Solid Earth* 105 (B2), 2969–2980.
- Zhu, L., Rivera, L.A., 2002. A note on the dynamic and static displacements from a point source in multilayered media. *Geophys. J. Int.* 148 (3), 619–627.